JOURNAL OF SOLID STATE CHEMISTRY 95, 365–387 (1991)

Studies of Rare Earth Cuprates with Structures Related to $NaCuO_2$

PETER K. DAVIES

Department of Materials Science and Engineering, University of Pennsylvania, 3231 Walnut St., Philadelphia, Pennsylvania 19104-6272

Received April 29, 1991

Solid solutions with structures based on an orthorhombic "$NaCuO_2$-type" subcell were formed over a wide range of composition in the CaO–M_2O_3–CuO systems, where M = Y, Nd, Gd. These structures contain infinite one-dimensional chains of edge-shared square planar cuprate groups crosslinked by the larger cations, which occupy sites in the inter-chain tunnels. Samples with $Ca/M \geq 1$ have the stoichiometry $Ca_{(2+x)}M_{(2-x)}Cu_5O_{10}$; the maximum solubility range corresponded to x = 0.8, 0.4, and 0.3 for M = Y, Gd, and Nd, respectively. Single phase samples with $Ca/M < 1$ were also formed in the Gd and Nd systems; these have the stoichiometry $M_{(10/3-y)}Ca_{(3y/2)}Cu_5O_{10}$, with $5/6 \leq y \leq 4/3$ for Nd and $1.13 \leq y \leq 1.33$ for Gd. Long-range ordered arrangements of the inter-chain ions lead to the formation of superstructures whose symmetry and periodicity is a sensitive function of the $Ca:M^{3+}$ ratio and the size of M. In general the superstructures are monoclinic and incommensurate along, and perpendicular to the cuprate chains. The ordering can be described in terms of a periodic displacive modulation of the inter-chain cations from their "ideal," equally spaced positions. Models based on a simple sinusoidal modulation give excellent agreement with experimental diffraction profiles collected using X rays and electrons.

1. Introduction

Recent studies on the CaO–M_2O_3–CuO (M = Nd, Gd, Y) systems have shown that the phase relations are dominated by a series of new layered cuprate phases with the nominal stoichiometry, $Ca_{(2+x)}M_{(2-x)}Cu_5O_{10}$ (*1*). The structures of these phases are closely related to that of $NaCuO_2$ (*2–4*) and the recently reported phase, $Ca_4Cu_5O_{10}$ (*2*). Compared to the binary compounds, these ternary phases can be prepared over a wide range of composition, with the detailed stoichiometry being dependent upon the chemistry of the trivalent ion. The X-ray patterns of these phases contain strong diffraction peaks that originate from commensurate and incommensurate, long-range ordered arrangements of the Ca and M ions in the structure. This paper reports on the results of detailed structural analysis of these new cuprates and presents evidence for an ordering mechanism involving displacive modulations of the Ca and M^{3+} atom positions.

Several cuprate phases have been reported to crystallize with structures containing infinite, one-dimensional chains of edge-shared square-planar cuprate groups. This class of closely related structures differs only through the cross-linking of the extended chains (*5*). The $NaCuO_2$ structure has recently received considerable attention due in part to its potential as a spectroscopic standard for Cu^{3+}. Though first reported by Hoppe as crystallizing in a triclinic space group (*6*), several groups have recently

0022-4596/91 $3.00

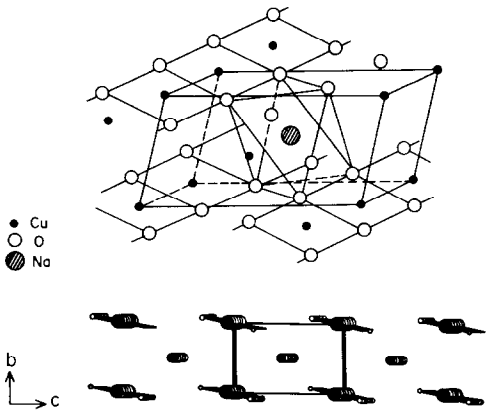

FIG. 1. Schematic views of the $NaCuO_2$ structure. Lower figure highlights the channels that crosslink the linear, edge-shared, one-dimensional chains of Cu square planes.

shown that this structure is monoclinic and contains parallel edge-shared $[CuO_2]$ chains linked by Na ions in octahedral coordination (*2–4*). A schematic view of the structure of $NaCuO_2$ is shown in Fig. 1. Aside from the linear edge-sharing $[CuO_2]$ chains, the primary crystal chemical feature of this phase is the inter-chain channel sites, which are fully occupied by the octahedrally coordinated Na ions. Closely related $ACuO_2$ phases are also formed for the other alkali metals. In the $KCuO_2$ (*3, 7*), Cs (*8*), and Rb (*9*) phases, the chains are displaced by half a polyhedron length and these larger alkali ions occupy the resultant trigonal prismatic sites. Similar structures have also been reported for the corresponding $MAuO_2$ phases; in the K phase the parallel chains are linked by cubic polyhedra (*9*).

Structural refinements of $Ca_4Cu_5O_{10}$ have shown that it is closely related to $NaCuO_2$ and contains similar extended $[CuO_2]$ chains (*2*). The packing arrangement of the cuprate chains in $Ca_4Cu_5O_{10}$ conforms to an orthorhombic subcell, space group *Fmmm*, as compared to the pseudo-orthorhombic symmetry of the sodium cuprate. In comparison to the alkali cuprates, this phase is cation deficient and the ordering of the calcium ions within the crosslinking channels leads to an orthorhombic, *Pnca* supercell in which the repeat distance along the chain direction, the *a* axis, is 5 times that of the corresponding subcell. The supercell repeat in this compound is largely dictated by the Ca–Ca distances; the Ca positions are equally spaced along the channels and adopt a distorted octahedral coordination (*2*).

The ternary $Ca_{(2+x)}M_{(2-x)}Cu_5O_{10}$ phases described in this paper crystallize with structures in which the subcell arrangement of the copper chains is identical to that reported for $Ca_4Cu_5O_{10}$ (*1*). However, the ordering of the Ca and trivalent ions in the sites that crosslink the linear cuprate chains is apparently more complex than that encountered in the pure calcium phase, and leads to the formation of commensurate and incommensurate superstructures. The results of powder X-ray diffraction and electron diffraction studies of the cation ordering in these phases are the subject of this paper.

2. Experimental Methods

The specimens in this study were prepared by standard solid state techniques by heating mixtures of Nd_2O_3 (or Gd_2O_3, Y_2O_3), $CaCO_3$, and CuO in the desired proportions. All the reagents were thoroughly dried before use and stored under appropriate desiccants. Typically 2 to 3 g of sample were heated slowly to 900°C for 12 hrs, reground and refired several times at 1000°C in air. The samples were fired in alumina boats lined with platinum foil. All the samples were investigated by powder X-ray diffraction (XRD) using an automated Rigaku DMaxB diffractometer with Cu$K\alpha$ radiation generated at 50 kV and 40 mA. X-ray patterns used to obtain lattice parameters were collected at scan speeds of 1 degree per minute using an internal standard. Least-

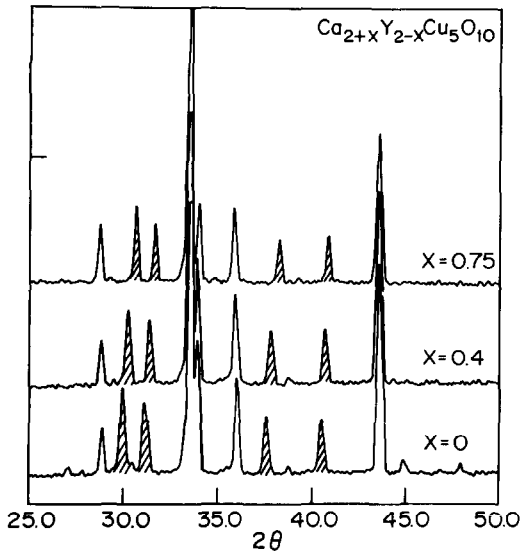

FIG. 2. Powder X-ray patterns of $Ca_{(2+x)}Y_{(2-x)}Cu_5O_{10}$ with $x = 0$, 0.4, and 0.75. Shaded peaks result from superstructure formation.

squares lattice parameter refinements and calculations of diffraction profiles were performed using FINAX programs. In certain cases the bulk oxygen content of the samples was determined by thermogravimetric analysis under forming gas (15% H_2/85% Ar). The samples were also investigated by Transmission Electron Microscopy (TEM). These specimens were ground under acetone and dispersed on to holey carbon grids in the usual manner. The TEM observations were made using a Philips 400T electron microscope operated at 120 kV.

3. Results

In the CaO–Y_2O_3–CuO system single phase samples with the general stoichiometry $Ca_{(2+x)}Y_{(2-x)}Cu_5O_{10}$ could be prepared with $0 \leq x \leq 0.8$, i.e., Ca : Y concentrations ranging from 1 : 1 to 2·33 : 1. The powder X-ray patterns of samples with $x = 0$, 0.4, and 0.75 are shown in Fig. 2. These patterns are characterized by one set of diffraction peaks whose positions are largely independent of x (these can be indexed in a routine manner using an orthorhombic cell, space group *Fmmm*) and by a second set of reflections whose positions, as indicated in the figure, vary considerably with x and cannot be indexed using conventional methods. For $x = 0$ the refined lattice parameters, $a = 2.817(1)$, $b = 6.185(1)$, $c = 10.594(1)$ Å, and the unit cell volume, $V = 184.63(7)$ Å^3, are almost identical to those reported by Siegrist *et al.* for the orthorhombic subcell of the low temperature phase $Ca_4Cu_5O_{10}$ (*2*). For all the compositions no evidence was found for any deviation of the subcell from orthorhombic symmetry. Compared to Na CuO_2, $Ca_4Cu_5O_{10}$ and the rare-earth cuprates discussed in this paper are cation deficient. As the following results will illustrate, the strong additional reflections observed in the powder patterns originate from commensurate and incommensurate ordering of the Ca/M^{3+} cations in the "channels" of the $NaCuO_2$-type cell.

Although the extra diffraction lines in the powder patterns cannot be indexed within the orthorhombic *Fmmm* cell, their positions, $d^* = ha^* + kb^* + lc^*$, can be indexed by retaining a^*, b^*, and c^* for the subcell and using noninteger values for h and l. Using fractional Miller indices based on the "$NaCuO_2$-type" orthorhombic subcell it is possible to fully index all the lines in the powder patterns of all the $Ca_{(2+x)}Y_{(2-x)}Cu_5O_{10}$ phases. For example, the two strong reflections observed close to $2\theta = 30°$ in the patterns in Fig. 2 can be indexed as $(1 - \delta a, 1, 1 - \delta c)$ and $(1 - \delta a, 1, 1 + \delta c)$, and two other major additional reflections close to $2\theta = 37°$ and 40° index as $(1 - \delta a, 1, 3 - \delta c)$ and $(1 - \delta a, 1, 3 + \delta c)$, respectively. Using this scheme the strongest superlattice reflections are observed for $(h - \delta a, k, l \pm \delta c)$ with h, k, l all odd. Having found a method for reliably indexing these patterns, the positions of the superstructure reflections were used to

TABLE I

INDEXING SCHEME FOR $Ca_2Y_2Cu_5O_{10}$

$2\Theta_{obs}$	$2\Theta_{calc}$	I_{rel}	h	k	l
16.65	16.73	7	0	0	2
28.85	28.84	14	0	2	0
29.83	29.84	25	$1 - \delta a$	1	$1 - \delta c$
31.03	31.04	20	$1 - \delta a$	1	$1 + \delta c$
33.53	33.53	100	0	2	2
33.81	33.83	33	0	0	4
35.99	36.00	22	1	1	1
37.53	37.50	18	$1 - \delta a$	1	$3 - \delta c$
40.37	40.40	17	$1 - \delta a$	1	$3 + \delta c$
43.61	43.59	42	1	1	3
45.03	45.04	3	0	2	4
50.65	50.61	12	$1 - \delta a$	1	$5 - \delta c$
51.73	51.74	9	$1 - \delta a$	3	$1 - \delta c$
51.73	51.76	4	0	.0	6
52.49	52.50	12	$1 - \delta a$	3	$1 + \delta c$
54.33	54.43	8	$1 - \delta a$	1	$5 + \delta c$
55.87	55.88	13	1	3	1
56.29	56.29	21	1	1	5
56.97	56.96	10	$1 - \delta a$	3	$3 - \delta c$
59.09	59.11	8	$1 - \delta a$	3	$3 + \delta c$
59.75	59.75	14	0	4	0
60.34	60.33	20	0	2	6
61.57	61.56	14	1	3	3

Note. a = 2.817(1), b = 6.185(1), c = 10.594(1) Å; δa = 0.2, δc = 0.25.

calculate δa and δc for each composition. For example, δc was evaluated from $\{1/d_{(1-\delta a,1,1-\delta c)^2} - 1/d_{(1-\delta a,1,1+\delta c)^2}\} = -4\delta_c/c^2$ and $\{1/d_{(1-\delta a,1,3+\delta c)^2}\} - 1/d_{(1-\delta a,1,3+\delta c)^2}\} = -12\delta_c/c^2$; δa was subsequently calculated from the positions of the individual lines. For samples with $x = 0$, i.e., $Ca_2Y_2Cu_5O_{10}$, $\delta a = 0.2$ and $\delta c = 0 \cdot 25$; this corresponds to a "commensurate" supercell with $a = 5a_{sub}$ = 14.092(4) Å, $b = b_{sub}$ = 6.185(1) Å, $c = 4c_{sub}$ = 42.36(1) Å. A complete indexing scheme for this compound is given in Table I. The same approach was used to index the X-ray patterns of the other compositions in the $Ca_{(2+x)}M_{(2-x)}Cu_5O_{10}$ system. As Ca is substituted for Y the supercells become incommensurate; for $x = 0.4$, $\delta a = 0.185$ and $\delta c = 0.248$, corresponding to a supercell with $a = 5.405a_{sub}$, $c = 4c_{sub}$, and for $x = 0.75$, $\delta a = 0.171$, $\delta c = 0.227$, giving a supercell with $a = 5.848a_{sub}$ and $c = 4.405c_{sub}$. A complete list of the sub- and supercell parameters is given in Table II.

To confirm the validity of the indexing methods described above, several samples were investigated using electron diffraction methods. Figure 3 shows a diffraction pattern of $Ca_2Y_2Cu_5O_{10}$ that was collected along the [010] zone axis of the subcell, which for all compositions was confirmed to be orthorhombic. Discrete satellite reflections are observed around each of the fundamental reflections, and these can all be indexed as $(h - 2n\delta a, 0, l - 2n\delta c)$. For example, around the transmitted beam the satellites correspond to $(2\delta a, 0, 2\delta c)$; for the (202) fundamental reflection the additional reflections can be indexed as $(2 - 2\delta a, 0, 2 - 2\delta c)$, and $(2 + \delta a, 0, 2 + 2\delta c)$. A schematic highlighting the satellite reflections observed in this zone is also presented in Fig. 3. The value of δa measured from this diffraction pattern is 0·2, with the a^* axis of the supercell being exactly 5 times smaller than the subcell. Much stronger satellites were observed in the [101] subcell zone axis patterns, see Fig. 4. In this pattern strong reflections along, for example, the $(h\ 1\ l)$ row occur at $(h \pm \delta a, 1, l \pm \delta c)$. The reflection at $(1 - \delta a, 1, 1 - \delta c)$ in particular is much stronger than the fundamental (111) spot originating from the subcell. This is consistent with the relative intensities observed in the powder X-ray patterns. The satellite reflections observed using this zone axis should only be allowed when $\delta a = \delta c$; measurements from the X-ray powder patterns and the electron diffraction patterns collected along [010] and other zones in fact show that $\delta a = 0.2$ and $\delta c = 0.25$; the observation of the formally forbidden satellites is primarily due to the c^* streaking that is quite evident in all these patterns.

Electron diffraction patterns were also collected along the [010] and [101] directions of $Ca_{(2+x)}Y_{(2-x)}Cu_5O_{10}$ samples with $x = 0.4$

TABLE II

STOICHIOMETRY RANGE, SUBCELL PARAMETERS AND SUPERCELL PERIODICITIES FOR $M_{(10/3-y)}Ca_{(3y/2)}Cu_5O_{10}$ AND $Ca_{(2+x)}M_{(2-x)}Cu_5O_{10}$

M	x	y	a_{sub}(Å)	b_{sub}(Å)	c_{sub}(Å)	V_{sub}(Å^3)	$1/\delta a$	$1/\delta c$	β(°)
Y	0.0	1.33	2.817	6.185	10.594	184.6	5.00	4.00	134.9
	0.4		2.827	6.206	10.581	185.6	5.41	4.03	137.4
	0.75		2.833	6.231	10.561	186.4	5.85	4.41	140.5
Nd		0.83	2.804	6.356	10.714	191.0	4.00	0.00	90.0
	0.0	1.33	2.825	6.356	10.689	191.9	4.76	5.71	136.1
	0.32		2.828	6.346	10.676	191.6	5.00	5.00	136.7
Gd		1.13	2.811	6.244	10.651	186.9	4.52	5.00	133.8
	0.0	1.33	2.822	6.251	10.642	187.8	4.88	4.57	135.3
	0.4		2.828	6.264	10.619	188.1	5.26	4.48	137.4

and $x = 0.75$. Strong satellite reflections were observed for both samples and could be indexed in the same manner as those for the $x = 0$ sample. In Fig. 5 the incommensurate repeat along the a^* axis is quite evident for both compositions. Direct measurements along the a^* direction yielded repeats of 5.6 and 5.84 for the 0.4 and 0.75 materials; these are in excellent agreement with those calculated from the X-ray patterns collected from the same powders. The strength of the supercell reflections observed in the [101] patterns were again comparable to many of the fundamental reflections; the resultant values of δc were in good agreement with those calculated from the X-ray indexing approach described above.

In the descriptions given above the supercells have been characterized in terms of the orthorhombic symmetry of the subcell; however, the positions and intensities of the satellites observed in the electron diffraction patterns show that the supercells are not orthorhombic but are of monoclinic symmetry. All the electron diffraction patterns can be re-indexed using monoclinic supercells, which are typically incommensurate with the orthorhombic subcell, with $a = a_{sub}\ 1/\delta a$, $b = b_{sub}$, $c = c_{sub}/\sin\beta$, where $\beta = 180° - \tan^{-1}\{(\delta a \times c_{sub})/(\delta c \times a_{sub})\}$. Table II shows the values for β, which increase with increasing Ca content. The monoclinic symmetry is further highlighted by the symmetry of the lattice fringes in images that were collected along the [010] directions of the three samples described above. Figure 6 shows an image collected from $Ca_2Y_2Cu_5O_{10}$. Direct measurements of the angles and spacing of the lattice fringes are consistent with an ordered monoclinic structure with $\beta \approx 135°$. Although the ordering along a is well defined and relatively free of defects, the structure is heavily twinned in the c direction. The microstructures of the samples with higher x values are equally disordered, see for example Fig. 7, which shows an image of the incommensurate ordered phase for $x = 0.75$.

Although the basic structure of the ternary phases in the Nd and Gd samples are the same as the Y system, distinct differences are observed in the details of the superlattice formation and in the stoichiometry range of the solid solution. Again samples with the stoichiometry $Ca_{(2+x)}M_{(2-x)}Cu_5O_{10}$ could be prepared at 1000°C, with the solid solution apparently moving toward the low temperature phase reported by Roth *et al.*, $Ca_4Cu_5O_{10}$ (*10*). The size of the orthorhombic subcell varied in accordance with the size of the trivalent ion, for example, for $Ca_2M_2Cu_5O_{10}$, $V_{subcell} = 191.9$

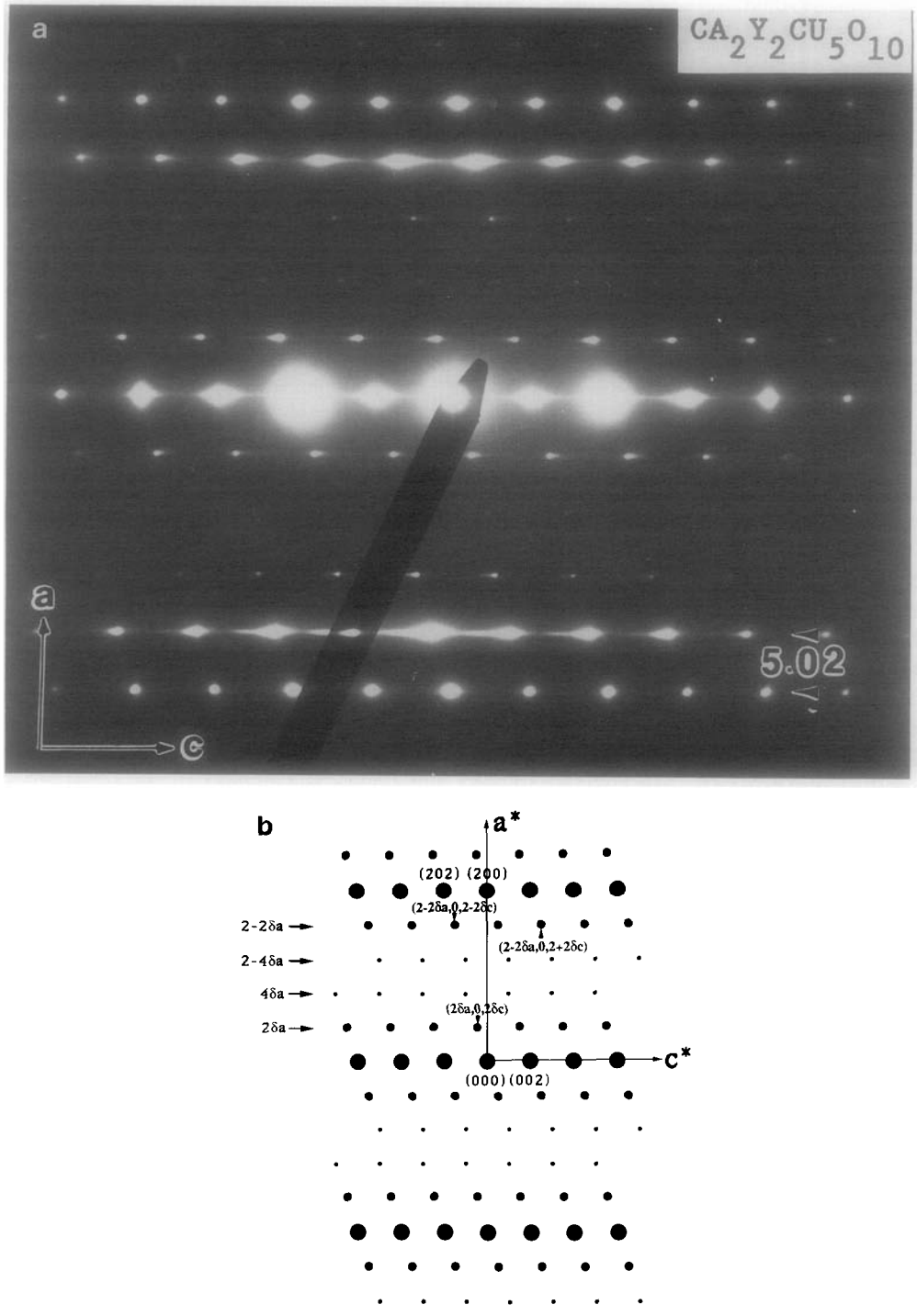

FIG. 3. (a) The [010] electron diffraction pattern collected from $Ca_2Y_2Cu_5O_{10}$; (b) schematic of this pattern highlighting the superlattice reflections.

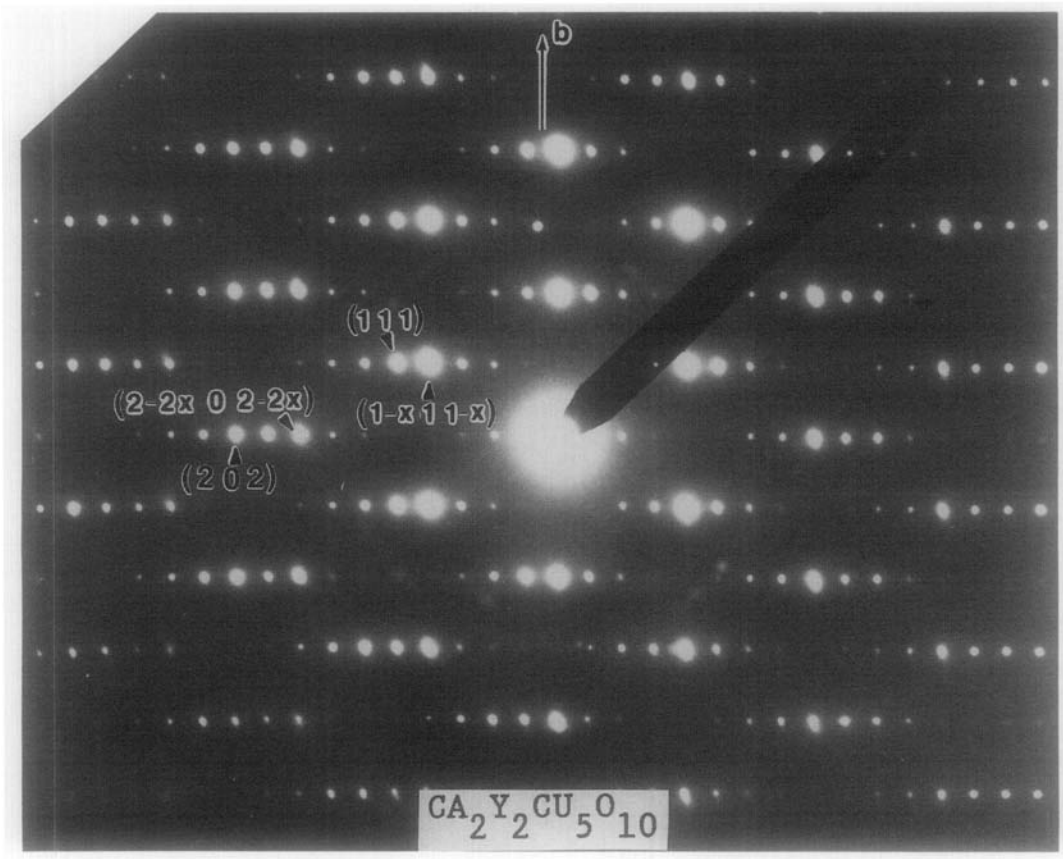

FIG. 4. The [101] pattern from $Ca_2Y_2Cu_5O_{10}$.

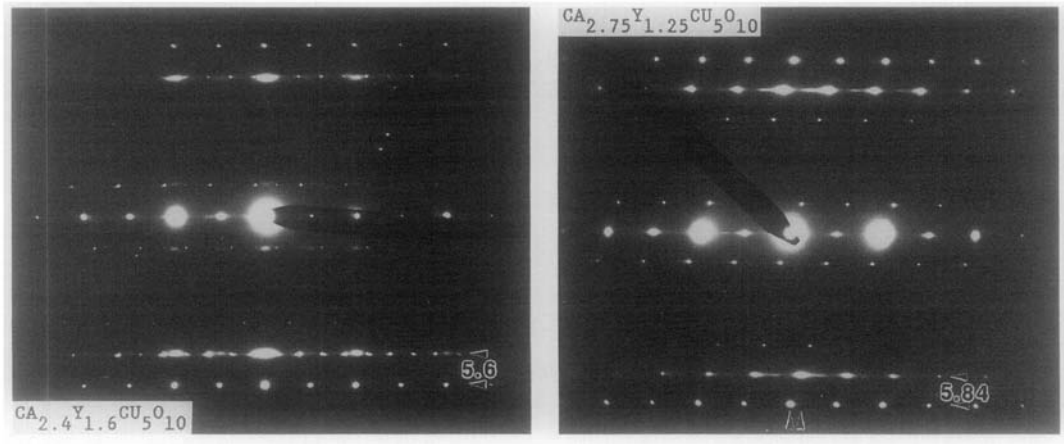

FIG. 5. The [010] diffraction patterns from $Ca_{(2+x)}Y_{(2-x)}Cu_5O_{10}$, $x = 0.4$ and 0.75.

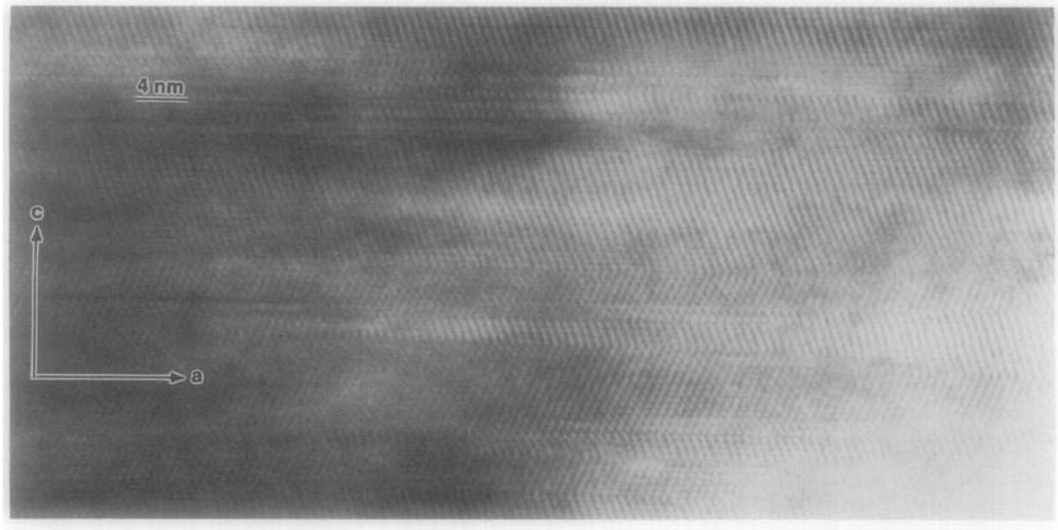

FIG. 6. The [010] lattice image of $Ca_2Y_2Cu_5O_{10}$.

Å^3 for Nd, 187.8 Å^3 for Gd, compared to 184.6 Å^3 for M = Y; see Table II for the complete set of lattice parameters. However, for positive values of x the range of the solution was found to decrease as the size of the trivalent ion increases, i.e., Y (x_{max} = 0.75) > Gd (x_{max} = 0.4) > Nd (x_{max} = 0.315). In all the Ca-rich samples the oxygen stoichiometry, as gauged by reduction experiments using TGA, remains constant, implying a partial stabilization of the 3^+ state for Cu.

In contrast to the Y system, it is possible to prepare trivalent-rich samples of the solid

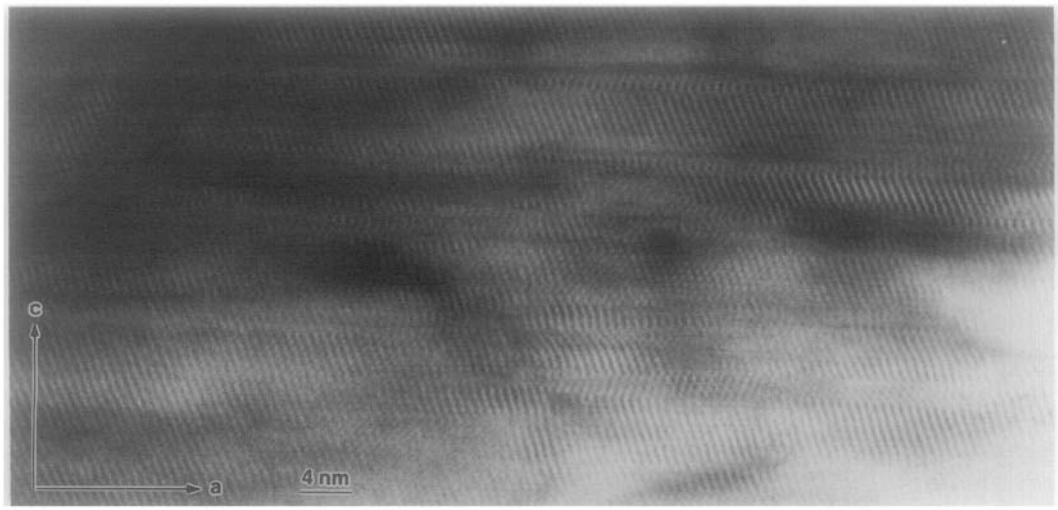

FIG. 7. The [010] lattice image from $Ca_{2.75}Y_{1.25}Cu_5O_{10}$.

solutions for M = Gd and Nd. In this region of the solid solution the overall composition deviates from the $Ca_{(2+x)}M_{(2-x)}Cu_5O_{10}$ stoichiometry, and the (Ca + M) : Cu content is <4 : 5. The composition of the solutions follows a stoichiometry that maintains copper in the divalent state, and the solutions proceed toward an hypothetical end-member, $M_{3.33}Cu_5O_{10}$, i.e., $M_2Cu_3O_6$. The stoichiometry in this range can be described by the general formula, $M_{(10/3-y)}Ca_{(3y/2)}Cu_5O_{10}$, and the degree of solution increases as the size of the trivalent ion increases; i.e., Nd > Gd (>Y), with $5/6 \leq y \leq 4/3$ for M = Nd, and $1{\cdot}13 \leq y \leq 1{\cdot}33$ for Gd. Clearly the concentration of (M + Ca) ions in the channels can only be reduced so far before the entire structure collapses. Therefore, it is not surprising that the dominant factor stabilizing the trivalent-rich samples is size, with the number of ions that can be "eliminated" from the channels being greater for the ions with the larger ionic radius.

The reduction in the total number of (M + Ca) ions has a pronounced effect on the variation of the lattice parameters of the subcell with composition, see Fig. 8. Samples of $Ca_{(2+x)}M_{(2-x)}Cu_5O_{10}$ with $x \geq 0$ retain the overall 4 : 5 (Ca + M) : Cu stoichiometry, and the lattice parameters and molar volume show a smooth, approximately linear variation with x. However, for $M_{(10/3-y)}Ca_{3y/2)}Cu_5O_{10}$ with $y \leq 4/3$, the compositional dependence of the subcell lattice parameters shows a distinct change, with a in particular becoming shorter as the M content is increased. In the Nd system, which exhibits the widest stoichiometry range in the trivalent-rich region, the volume increases with y up to the 2 : 2 stoichiometry, primarily because of the increase in a; above the 2 : 2 composition, where the solution retains a 4 : 5 stoichiometry, the molar volume decreases with increasing x, presumably because of the increase in the concentration of Cu^{3+}.

In general, the X-ray patterns for the Ca-rich samples in the Nd and Gd systems are similar to those observed for the Y system; however, the positions of the additional diffraction lines originating from the formation of the superstructure show a pronounced change as the compositions become trivalent-rich. Figure 9 illustrates the variation of the d spacings with the Ca : M ratio for several fundamental subcell and superlattice reflections in the Nd system. As the concentration of Nd is increased beyond a 1 : 1 Ca : Nd content, the splitting between the pairs of ($h - \delta a$, k, $l - \delta c$), and ($h - \delta a$, k, $l + \delta c$) reflections decreases; this corresponds to a decrease in δc and therefore a decrease in β for the monoclinic supercell. At the solubility limit, $Nd_{2.5}Ca_{1.25}Cu_5O_{10}$ or $Nd_2CaCu_4O_8$, these lines merge, $\delta c = 0$, and a commensurate, orthorhombic supercell is formed with $\delta a = 0.25$, i.e., $a = 4a_{sub}$, $b = b_{sub}$, and $c = c_{sub}$. The complete x-ray pattern for this sample is shown in Fig. 10, and Table III gives a list of the d spacings and the corresponding indices with respect to both the sub- and supercells. In Fig. 11 the [010] electron diffraction patterns of a sample close to the end-member composition confirm this indexing scheme and the superlattice reflections are observed at ($h - \delta a$, 0, l) for $\delta a = 0.25$ with h and $l = 2n$. As Ca is substituted for Nd, the supercells become monoclinic, and the X-ray patterns can be indexed in the same manner as the Y system.

Table II shows the calculated δa and δc values for the $x = 0$ and Ca-rich end-member compositions in the Nd system, and the supercells in the Gd system. It is interesting to note that for the "stoichiometric composition" $Ca_2M_2Cu_5O_{10}$, the supercells for both Nd ($a = 4.76a_{sub}$, $c = 5.714c_{sub}$) and Gd ($a = 4.88a_{sub}$, $c = 4.57c_{sub}$) are incommensurate, whereas a "commensurate" supercell ($a = 5a_{sub}$, $c = 4c_{sub}$) is observed for this composition in the Y system. The superstructure of the divalent-rich end-member of the Nd solid solution,

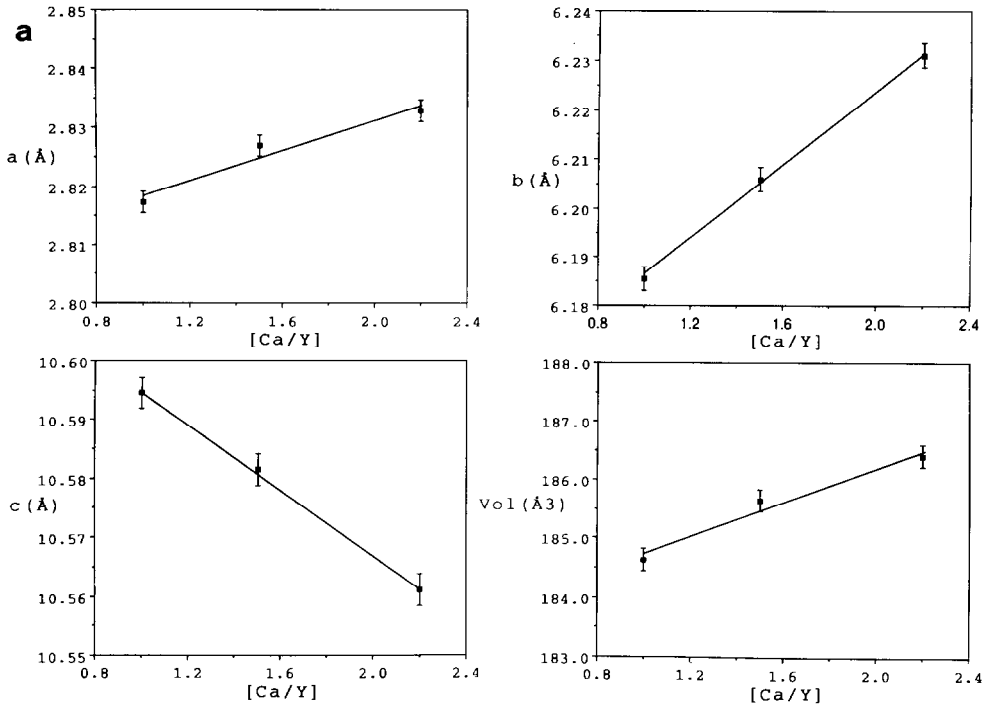

FIG. 8. Subcell lattice parameters for $Ca_{(2+x)}M_{(2-x)}Cu_5O_{10}$ Systems: (a) M = Y, (b) M = Gd, and (c) M = Nd.

$Ca_{2.315}Nd_{1.685}Cu_5O_{10}$, is apparently commensurate with the subcell and $\delta a = \delta c = 0.2$. The positions of all the lines in the X-ray powder pattern of this sample can be successfully indexed and refined within the corresponding $P2_1/c$ monoclinic supercell, and $a = 5a_{sub} = 14.138(3)$ Å, $b = 6.348(1)$ Å, $c = c_{sub}/\sin\beta = 15.554(3)$ Å, $\beta = 180° - \tan^{-1}\{(\delta a \times c_{sub})/(\delta c \times a_{sub})\} = 136.55(1)°$, see Table IV. The details of the structural features of this supercell are discussed in the following section. Again the superstructure for a given composition is dependent upon the chemistry of M, and the corresponding composition in the Y system, $Ca_{2.315}Y_{1.685}Cu_5O_{10}$, has an incommensurate superlattice with $a = 5.35a_{sub}$, $c = 4.03c_{sub}$.

Finally, to explore the response of these systems to changes in the chemistry of the divalent ion, a series of samples with the stoichiometry $Nd_2(Ca_{2-z}Sr_z)Cu_5O_{10}$ were examined. At 1000°C single phase samples could be prepared for $0 \leq z \leq 0.3$. As expected, the subcell for $Nd_2Ca_{1.7}Sr_{.3}Cu_5O_{10}$, is larger, $a = 2.824(1)$ Å, $b = 6.395$ Å (2), $c = 10.721(3)$ Å, $V = 193.6$ Å^3, than the corresponding sample with $z = 0$, where $a = 2.825$ Å, $b = 6.356$ Å, $c = 10.689$ Å, $V = 191.9$ Å^3. However, the substitution of Sr for Ca does not change a, which is largely constrained by the Cu–O distance, but does expand b and c. Analysis of the supercell reflections shows that the superlattice repeat along a is also insensitive to the size of the divalent ion, $\delta a = 0.21$, but the correlations along c change considerably; for $z = 0.3$, $\delta c = 0.14$, as compared to $\delta c = 0.175$ for $z = 0$.

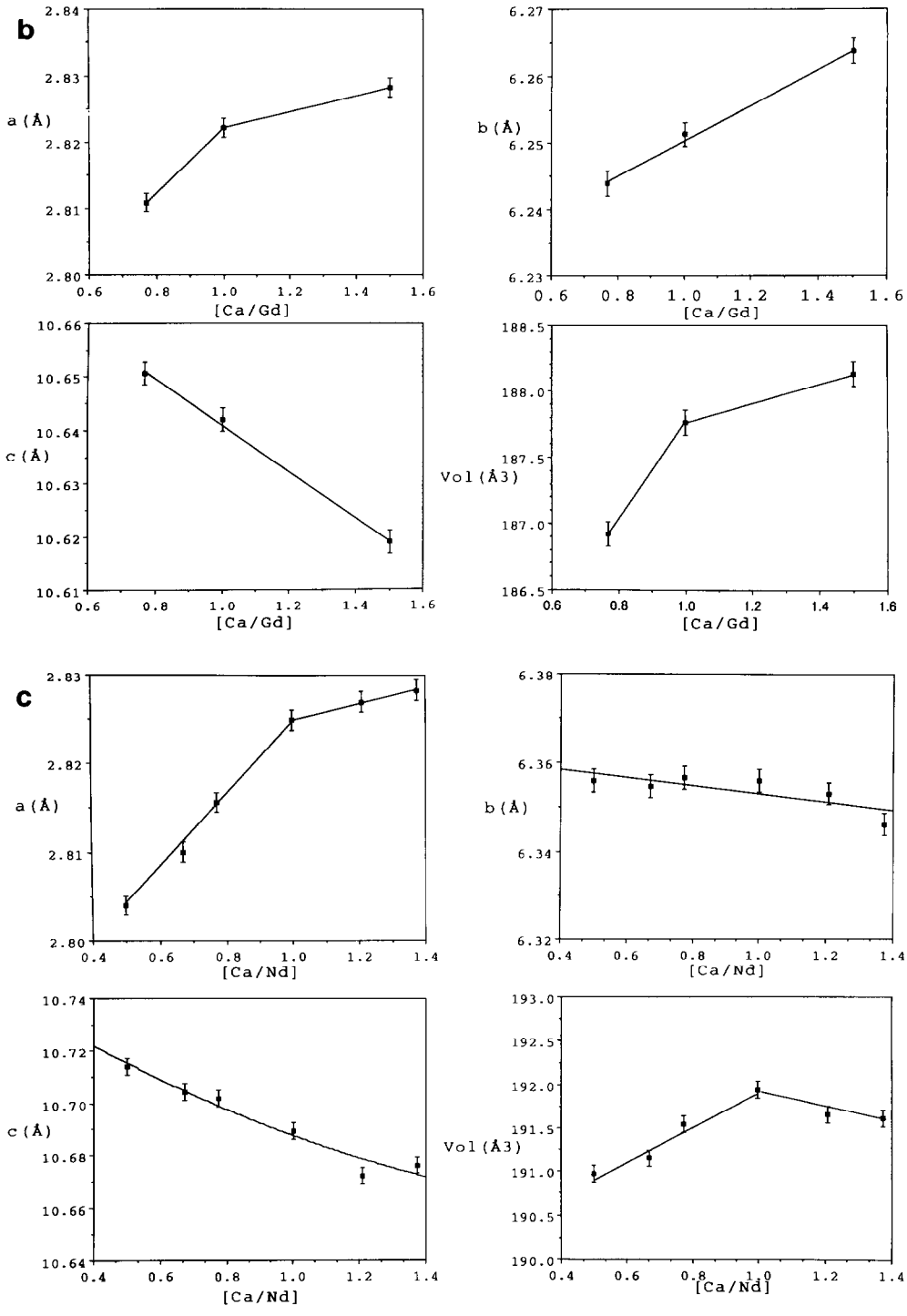

FIG. 8—*Continued*

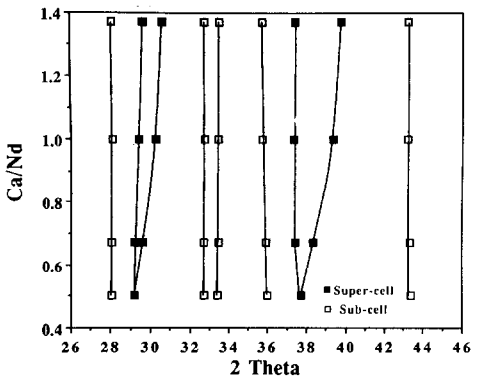

FIG. 9. Variation of the positions of the major sub- and supercell reflections with composition in the Nd system.

TABLE III

INDEXING SCHEME FOR $Nd_2CaCu_4O_8$

$2\Theta_{obs}$	$2\Theta_{calc}$	I_{obs}	I_{calc}	h_{sub}	k_{sub}	l_{sub}	h_{sup}	k_{sup}	l_{sup}
16.50	16.53	9	5	0	0	2	0	0	2
28.04	28.07	8	3	0	2	0	0	2	0
29.15	28.98	46	83	$1-\delta a$	1	1	3	1	1
32.73	32.75	100	100	0	2	2	0	2	2
33.43	33.41	33	28	0	0	4	0	0	4
35.95	36.07	16	14	1	1	1	4	1	1
37.77	37.61	30	38	$1-\delta a$	1	3	3	1	3
43.40	43.48	35	32	1	1	3	4	1	3
44.19	44.18	8	3	0	2	4	0	2	4
50.31	50.24	23	14	$1-\delta a$	3	1	3	3	1
51.18	51.44	15	13	$1-\delta a$	1	5	3	1	5
51.92	51.44	15	6	$2-2\delta a$	0	2	6	0	2
54.97	55.04	11	5	1	3	1	4	3	1
55.86	55.92	19	13	1	1	5	4	1	5
56.12	56.16	13	9	$1-\delta a$	3	3	3	3	3
57.25	57.29	9	4	$2-2\delta a$	2	0	6	2	0
58.00	58.02	16	10	0	4	0	0	4	0
59.31	59.30	20	14	0	2	6	0	2	6

Note. Subcell: a = 2.804(1), b = 6.356(1), c = 10.714(1) Å, δa = 0.25, δc = 0.0. *Acaa* supercell: a = 11.170(30), b = 6.351(8), c = 10.720(18) Å.

4. Discussion

Solid solutions with structures based on an orthorhombic "$NaCuO_2$-type" subcell can be formed over a wide range of composition in the CaO–M_2O_3–CuO systems. Compositions with $Ca/M \geq 1$ have the stoichiometry $Ca_{(2+x)}M_{(2-x)}Cu_5O_{10}$, and form a partial solid solution with the Ca end-member, $Ca_4Cu_5O_{10}$. Although the pure Ca compound can be formed below 750°C (*10*) under the conditions of this study, 1000°C in air, the maximum solubility range corresponded to $x = 0.8$ for M = Y; $x = 0.4$ for Gd; and $x = 0.31$ for Nd. In this region the formal oxidation state of copper is higher than 2, however all these samples remain insulating. The lower oxidation state of Cu in the ternary compounds is consistent with their increased thermal stability as compared to $Ca_4Cu_5O_{10}$ and $NaCuO_2$, which can only be prepared below 750 and 500°C, respectively. Single phase compositions with $Ca/M < 1$ are also formed in the Gd and Nd systems with the stoichiometry $M_{(10/3-y)}Ca_{(3y/2)}Cu_5O_{10}$, and a hypothetical end-member $M_2Cu_3O_6$. For Nd $5/6 \leq y \leq 4/3$ and for Gd $1.13 \leq y \leq 1.33$. In this trivalent-rich region the (Ca + M) : Cu concentration systematically decreases as y decreases, and the copper ions remain in the divalent state. This discussion begins with a consideration of the homogeneity range of these systems.

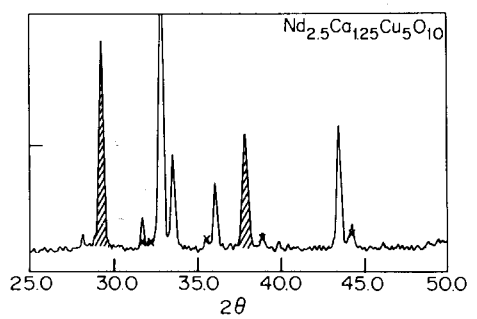

FIG. 10. Powder X-ray pattern of $Nd_2CaCu_4O_8$, or $Nd_{2.5}Ca_{1.25}Cu_5O_{10}$. Commensurate superlattice peaks are shaded. Small impurity peaks from Nd_2CuO_4 and CuO are indicated by X.

The extent of solid solubility in the trivalent-rich regions appears to be primarily governed by size considerations, and the solubility limit increases with the size of the trivalent ion. As the concentration of M^{3+} increases, the inter-chain channels become increasingly depleted in the large cations,

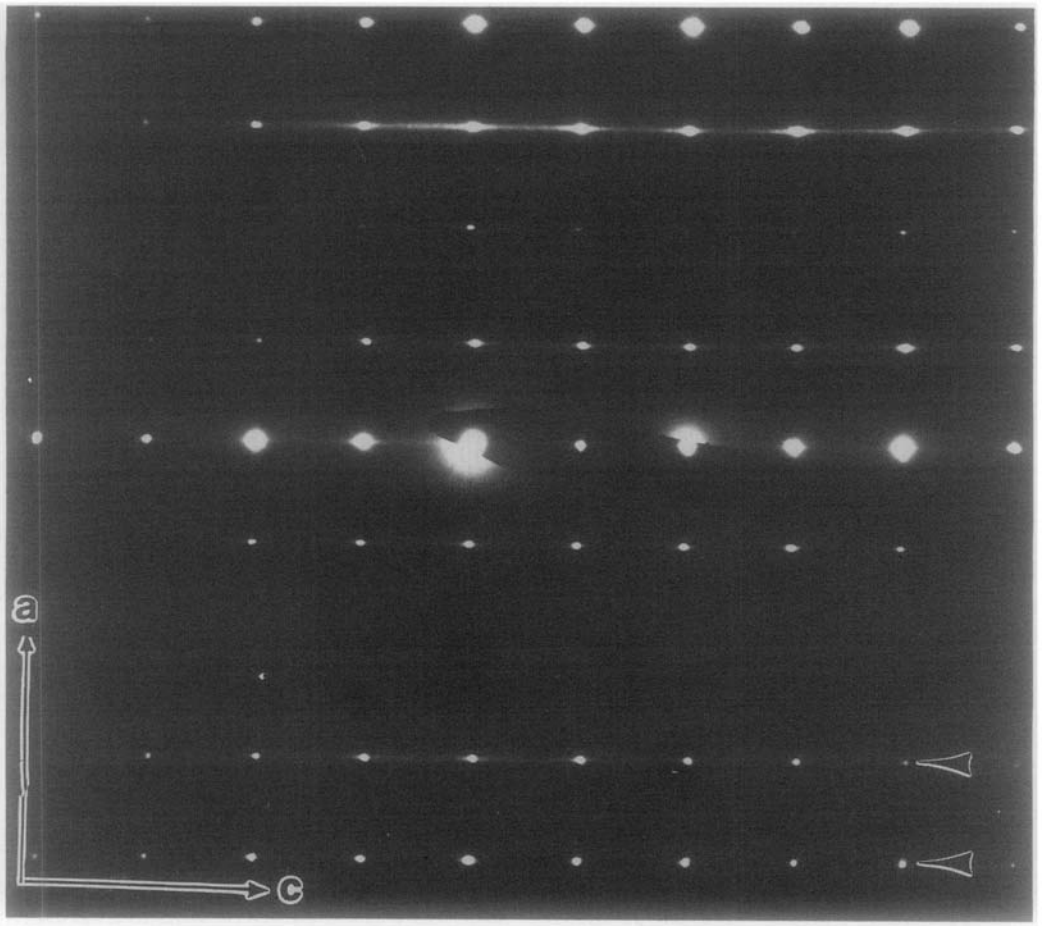

FIG. 11. The [010] electron diffraction patterns collected from a sample with a composition close to $Nd_2CaCu_4O_8$.

and the structural stability would be expected to decrease. Apparently for the smaller Y^{3+} ions the number of inter-channel ions cannot be reduced below the value of 0·8 per Cu observed in $Ca_2Y_2Cu_5O_{10}$, and no Y-rich samples could be prepared. Conversely, for the larger Nd ions the structure can accommodate significant reductions in the number of cations in the channels, and it is possible to decrease the (Ca + M^{3+}) : Cu concentration to 0·75.

The change in the concentration of the inter-channel ions from 4 : 5 in the Ca-rich samples to <4 : 5 in the trivalent-rich compositions is reflected by the variation of the subcell lattice parameters with the Ca : M concentration. The subcell parameters for $M_{(10/3-y)}Ca_{(3y/2)}Cu_5O_{10}$ show a smooth linear variation with y; similarly, a, b, c, and V vary linearly for the Ca/M > 1 region as the divalent ion concentration is increased, see Fig. 8. However, as the composition moves below the $x = 0$, or $y = 4/3$ boundary, the most noticeable change is the rapid decrease in a as the M^{3+} content is increased.

The depletion in the number of crosslinking ions in the channels ensures that the copper ions remain in the divalent state in

TABLE IV

INDEXING SCHEME FOR $Ca_{2.315}Nd_{1.685}Cu_5O_{10}$

$2\Theta_{obs}$	$2\Theta_{calc}$	I_{obs}	I_{calc}	h_{sub}	k_{sub}	l_{sub}	h_{sup}	k_{sup}	l_{sup}
16.55	16.59	1	2	0	0	2	0	0	2
28.10	28.09	7	6	0	2	0	0	2	0
29.68	29.67	30	35	$1 - \delta a$	1	$1 - \delta c$	4	1	−4
30.65	30.62	24	32	$1 - \delta a$	1	$1 + \delta c$	4	1	−2
32.79	32.80	100	100	0	2	2	0	2	2
33.56	33.55	32	26	0	0	4	0	0	4
35.73	35.74	19	15	1	1	1	5	1	−5
							5	1	−3
37.45	37.44	17	18	$1 - \delta a$	1	$3 - \delta c$	4	1	−6
39.75	39.74	15	15	$1 - \delta a$	1	$3 + \delta c$	4	1	0
43.24	43.24	44	38	1	1	3	5	1	−7
							5	1	−1
44.31	44.31	4	3	0	2	4	0	2	4
50.53	50.63	14	7	$1 - \delta a$	1	$5 - \delta c$	4	1	−8
50.71	50.63		7	$1 - \delta a$	3	$1 - \delta c$	4	3	−4
51.33	51.32	10	6	$1 - \delta a$	3	$1 + \delta c$	4	3	−2
53.57	53.56	8	6	$1 - \delta a$	1	$5 + \delta c$	4	1	2
53.57	53.60		3	$2 - 2\delta a$	0	$2 - \delta c$	8	0	−8
54.82	54.82	4	4	1	3	1	5	3	−5
							5	3	−3
55.84	55.82	13	15	1	1	5	5	1	−9
							5	1	1
58.10	58.08	25	12	0	4	0	0	4	0
59.51	59.51	18	14	0	2	6	0	2	6

Note. Subcell: $a = 2.828(1)$, $b = 6.346(1)$, $c = 10.676(2)$ Å, $\delta a = 0.2$, $\delta c = 0.2$. $P2_1/c$ supercell: $a = 14.138(3)$, $b = 6.348(1)$, c 15.554(3) Å, $\beta = 136.65(1)°$.

the M^{3+}-rich regions; however, for the calcium-rich compositions the total number of channel ions remains constant, and the valence of copper increases as Ca is substituted for M. A maximum Cu valence of 2.16^+ is observed for the Ca-rich end-member in the Y system. In contrast to the trivalent-rich region, the extent of the solid solution on this side of the system is inversely proportional to the size of the trivalent ion. From size arguments alone this is somewhat surprising, considering that in most substitutional solid solutions the solubility decreases as the difference in the size of the ions being mixed increases (*11*). Given the ionic radii of the octahedrally coordinated ions (*12*), Ca = 1.0 Å, Y = 0.9 Å, Nd = 0.983 Å, Gd = 0.938 Å, size factor arguments alone would favor maximum substitution of Ca in the Nd system and minimum solubility in the Y system. Similarly, consideration of the expected stability of Cu^{3+} in the three systems does not explain the observed substitution limits. Generally, high copper valences are stabilized in systems containing highly electropositive or basic cations such as the alkalis or alkaline earths. This general rule is followed in these particular systems by the formation of the stable trivalent copper compounds $NaCuO_2$ and $KCuO_2$. In these cases the increase in "the effective ionicity" of the M–O bond tends to increase the covalency of the corresponding Cu–O bonds stabilizing the formal Cu^{3+} state. However, these simple electronegativity arguments would predict that the stability of Cu^{3+}, and therefore the extent of solid solution, would increase in the order Nd > Gd > Y. Again this contradicts the experimental results. One other possible explanation for the variation in the degree of solution in these three systems could be related to differences in the local coordination of the divalent and trivalent ions in the channels. In the ideal subcell structure, the least distorted octahedral sites are located at $x = 0.25$ and $x = 0.75$. The refined Ca positions in $Ca_4Cu_5O_{10}$, which have high thermal factors and are subject to considerable uncertainty, are displaced from these positions and, although they are 6-coordinate, occupy significantly distorted sites. To explain the differences in the stoichiometry range of the $Ca_{(2+x)}M_{(2-x)}Cu_5O_{10}$ systems, it is possible that at a local level the trivalent ions are able to significantly polarize their oxygen nearest neighbors, and occupy either sites that approach more regular octahedral coordination or sites with a higher coordination that approaches local 8-fold or cubic symmetry. It seems reasonable to expect that the ability of the trivalent ions to displace the nearest neighbor anions and increase their local coordination should scale with their size and electronegativity, i.e., Nd > Gd > Y. If the site preference of the trivalent ions varies in this manner, it makes sense that the substitution of Ca for a cation with a lower specific site preference, such as Y, should be more

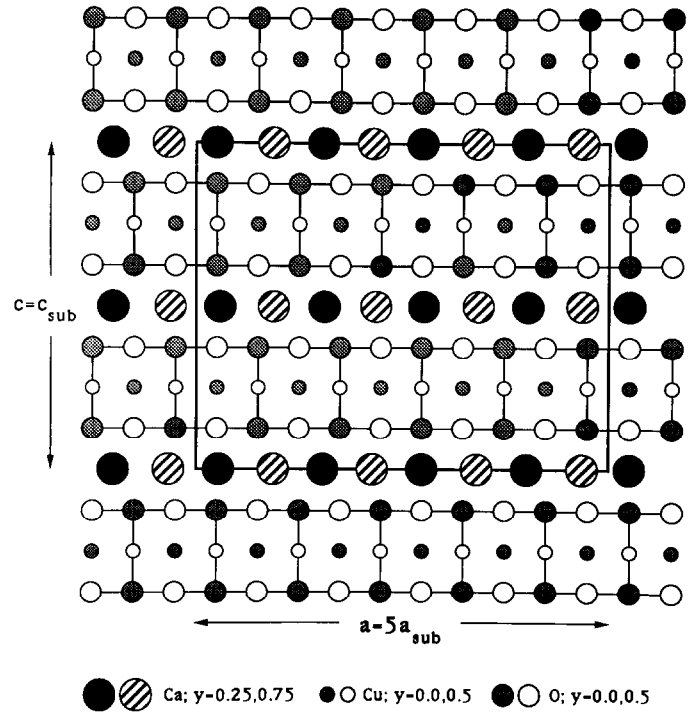

FIG. 12. Schematic [010] projection of the $Ca_4Cu_5O_{10}$ structure; $a = 5a_{sub}$, $b = b_{sub}$, and $c = c_{sub}$.

favorable than substitution for a higher "site specific" ion such as Nd. This argument regarding the importance of the local trivalent coordination is also addressed below in the consideration of the superstructure formation in these systems.

Previous work on the $Ca_4Cu_5O_{10}$ system showed that the long-range ordering of the Ca ions is dominated by the equilibrium cationic separations within the channels rather than by specific site preferences (*2*). In that work, which utilized single crystal X-ray diffraction, the supercell was commensurate along a, $\delta a = 0.2$, and along c, $\delta c = 0$. The ideal site positions, which lead to equal cation–cation distances of 3.51 Å, are shown schematically in Fig. 12. Again it should be noted that the large thermal factors reported for both the Ca and O ions indicate the possibility of significant local displacements in the atom positions, and although the $Ca_4Cu_5O_{10}$ crystal used in that study was orthorhombic, monoclinic superstructures were observed, though not refined, for other crystals of the same nominal composition. The ternary phases reported in this work have the same orthorhombic subcell arrangement as $Ca_4Cu_5O_{10}$, but the periodicity of the supercell along both the a and c axes of the subcell is a sensitive function of composition. The satellite reflections that are observed for these oxides could result from either a displacive or substitutional modulation in which the position or chemical occupancy, or both, vary between the unit cells of the substructure along the a and c axes. For most compositions $1/\delta a$ and $1/\delta c$ are not simple multiples of a or c; the ordering modulation is incommensurate, and therefore the structure cannot generally be described using a superstructure cell that is a simple multiple of the subcell.

TABLE V

IDEAL ATOM POSITIONS FOR $Nd_2Ca_1Cu_4O_8$

Atom	x	y	z	occup.
Cu1	0.9375	0.0	0.25	1.0
Cu2	0.6875	0.0	0.25	1.0
Ca1	0.25	0.25	0.0	0.33
Nd1	0.25	0.25	0.0	0.67
Ca2	0.9167	0.25	0.0	0.33
Nd2	0.9167	0.25	0.0	0.67
O1	0.8125	0.0	0.125	1.0
O2	0.9375	0.5	0.125	1.0

Note. Space group *Acaa*, $a = 11.170$, $b = 6.351$, $c = 10.721$ Å.

With respect to $NaCuO_2$, the ternary and $Ca_4Cu_5O_{10}$ phases are cation deficient, and the periodicities of the superstructures seem to be determined by the equilibrium Ca^{2+}–Ca^{2+}, Ca^{2+}–M^{3+}, and M^{3+}–M^{3+} separations within the crosslinking channels of the structure. Additional modulations of the Cu and O atom positions to accommodate the location of the channel ions cannot be ruled out, and indeed would be expected. Generally, the superstructures are monoclinic rather than orthorhombic, with $a = a_{sub}\ 1/\delta a$, $b = b_{sub}$, $c = c_{sub}/\sin \beta$, where $\beta = 180° - \tan^{-1}\{(\delta a \times c_{sub})/(\delta c \times a_{sub})\}$. For certain compositions the supercells are commensurate with the structure of the subcell. To gain some insight into the nature of the long-range order, the diffraction profiles of these supercells were modeled using conventional 3-*d* space groups. For the Nd-rich end-member, $Nd_2CaCu_4O_8$ with $\delta a = 0.25$ and $\delta c = 0$, the positions of all the reflections in the X-ray pattern can be indexed using a supercell with $a = 4a_{sub}$, $b = b_{sub}$, $c = c_{sub}$, see Table III. The intensities of these reflections were calculated using a space group Acaa and the atom positions listed in Table V. In this model the cations were placed at sites that lead to equal separations of all the cations in each channel, see Fig. 13. For example, atoms at $y = 0.25$ were placed at $x = 3/12$, 7/12, and 11/12, with cation–cation distances of $1.33a_{sub} = 3.73$ Å. The intensities calculated using FINAX are shown in Table III; considering that no attempt was made to perform a full profile analysis, these are in very good agreement with those determined experimentally. The intensities were calculated assuming random occupancy of Nd and Ca in the 4*a* and 8*g* atom sites; additional reflections resulting from Nd–Ca order, perhaps via the formation of [–Ca–Nd–Nd–Ca–] chains along *a*, were not observed in the powder X-ray patterns. However, evidence for this type of local order, which would certainly be expected on electrostatic grounds, was found in the electron diffraction patterns of $Nd_2Ca Cu_4O_8$. For example, the patterns collected along the [010] direction in Fig. 11 show superlattice reflections at $h = \pm 2\delta a$, $\pm 4\delta a$, and $2 \pm 2\delta a$; only $2 \pm 2\delta a$ is expected for a random Nd/Ca distribution, whereas all these reflections should be observed for an ordered channel ion arrangement with Ca in the 4*a* sites and Nd in the 8*g* sites.

When the Ca content in $M_{(10/3-y)}Ca_{(3y/2)} Cu_5O_{10}$ is increased from $y = 5/6$ in $Nd_2Ca Cu_4O_8$, to $y = 1.33$ in $M_2Ca_2Cu_5O_{10}$ (M = Nd, Gd), the periodicity of the supercell along the channels increases linearly from $\delta a = 0.25$ to $\delta a \approx 0.2$; δc adopts values that are dependent upon the size of M^{3+}; for $y = 1.33$, $\delta c = 0.219$ with M = Gd and 0.175 for Nd. If the magnitude of the modulation along the channels was solely related to substitutional effects, one would expect a simple relationship between δa and the total number of channel atoms per Cu ion, i.e., $\{(10/3 + y/2)/5\}$. For the Nd end-member, $Nd_2CaCu_4O_8$ ($y = 5/6$), $\Sigma(Ca + Nd)/Cu = 0.75$, and the smallest repeat that leads to a cell with an integer number of ions is 4, i.e., $\delta a = 0.25$. Similarly for $Nd_2Ca_2Cu_5O_{10}$ ($y = 1.33$), $\Sigma(Ca + M)/Cu = 0.8$, the smallest supercell that contains an integer number of channel atoms has $a = 5a_{sub}$, i.e.,

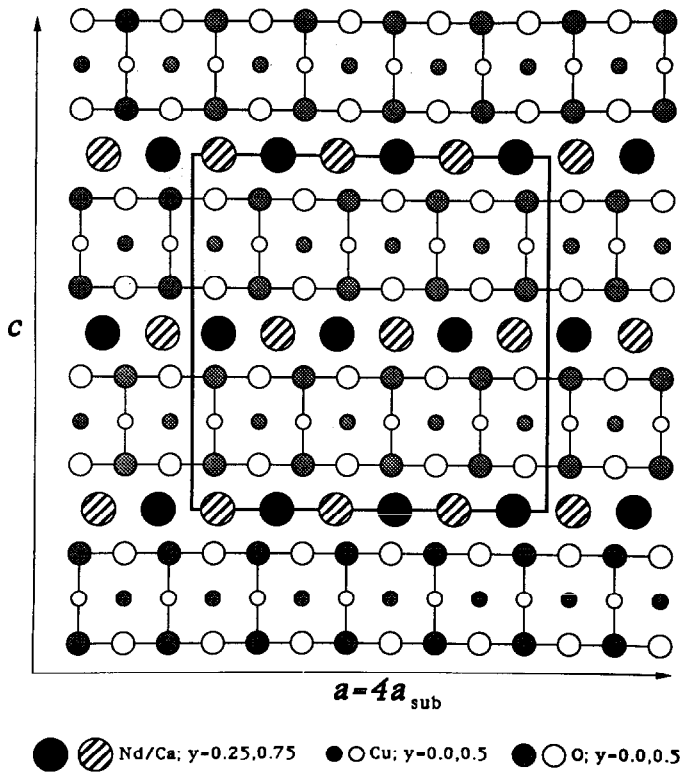

FIG. 13. Ideal cation positions in $Nd_2CaCu_4O_8$; $a = 4a_{sub}$, $b = b_{sub}$, and $c = c_{sub}$.

$\delta a = 0.2$. However, for the intermediate compositions the superstructures predicted from this simple "substitutional" model do not agree with those observed experimentally. For a composition with $y = 13/12$, $M_{2.25}Ca_{1.625}Cu_5O_{10}$, where $\Sigma(M + Ca)/Cu = 3.875/5 = 0.775$, the observed supercell has $\delta a = 0.225$. If the modulation was simply a result of a cation arrangement with equally separated cations, a supercell containing an integer number of ions would have a periodicity (n/0·775), where n is the total number of ions in the repeat unit; e.g., for $n = 4$, $\delta a = 0.194$; $n = 3$, $\delta a = 0.26$, etc. Alternatively, if the period of the modulation is determined primarily by the separation and number of trivalent ions in the channels, i.e., $(M^{3+}/Cu) = (10/3 - y)/5$, then the expected repeat for a cell containing an integer number of M^{3+} atoms would be given by $5n/(10/3 - y)$. For $y = 13/12$ and $n = 2$ this yields a periodicity with $\delta a = 0{\cdot}225$, which is consistent with that observed experimentally, and for this supercell the composition can be written as $Nd_2Ca_{1.444}Cu_{4.444}O_{8.88}$.

The relationship between the periodicity of the modulation and the trivalent ion content, rather than the total cation content or the Ca concentration, once again highlights the apparent importance of the trivalent positions in these systems. Furthermore, this correlation indicates that all the cation–cation distances in the channels cannot be equal and may provide support for a displacive, rather than substitutional, structural modulation in which the cation positions are displaced away from their "ideal" positions

in a regular manner. Clearly a complete treatment of an incommensurate modulation is beyond the scope of the diffraction results obtained in this work, and given the large degree of microtwinning in all these samples, these structures could not be treated reliably by any diffraction analysis. However, it is possible to extract some useful insight into the chemistry of these systems by assuming that the superstructures result from a simple sinusoidal displacement of the atoms from their ideal positions. Using this approach, further confirmation of the displacive nature of the superstructures is provided by consideration of the periodicities in samples of the Ca-rich solutions.

For the Ca-rich compositions the stoichiometries correspond to $Ca_{(2+x)}M_{(2-x)}Cu_5O_{10}$ and within the limits of our studies we found no evidence for any significant deviation from a [Ca + M]/Cu ratio of 4 : 5. Although the total concentration of the channel ions in this region is constant, the period of the modulation along a^* is not, and δa is dependent upon the Ca : M content and the nature of M. For example, for M = Y, δa varies linearly from 0.2 at $x = 0$, to 0.171 for $x = 0.75$; however, for samples with $x = 0.315$, $\delta a = 0.187$ for M = Y, whereas for M = Nd, $\delta a = 0.2$. It seems impossible to describe these variations in the period of the modulation by any scheme involving a substitutional mechanism. Again the superlattice repeats probably reflect the periodicity of a displacive modulation which is a sensitive function of the local cation–cation distances, in particular the Ca^{2+}–Ca^{2+} and Ca^{2+}–M^{3+} interactions that predominate in this region, and therefore the size/chemistry of M^{3+} as well as the M : Ca concentration.

Figure 14 shows a schematic representation of a proposed structural model for $Ca_{(2+x)}M_{(2-x)}Cu_5O_{10}$ with $x = 0.315$ and M = Nd. This composition represents the solubility limit for the Nd system, and the modulations along a and c are "commensurate" with the orthorhombic subcell, $\delta a = \delta c = 0.2$. For this sample the monoclinic supercell is also commensurate with the orthorhombic subcell. Least-squares refinement of the observed reflections in the X-ray patterns within a $P2_1/c$ space group, yields a supercell with $a = a_{sub}\ 1/\delta a = 14.138(3)$, $b = b_{sub} = 6.348(1)$, $c = c_{sub}/\sin\beta = 15.554(3)$ Å, where $\beta = 180° - \tan^{-1}\{(\delta a \times c_{sub})/(\delta c \times a_{sub})\} = 136.65(1)°$, see Table IV. The intensities were calculated for this cell assuming the Ca and Nd atoms occupy "ideal", equally spaced positions along the a axis; i.e. for $z = 0$, $x = 1/16$ ($5/16x_{sub}$), 5/16 ($25/16x_{sub}$), 9/16 ($45/16x_{sub}$), 13/16 ($65/16x_{sub}$), for $y = 0.25$; and $x = 3/16$ ($15/16x_{sub}$), 7/16 ($35/16x_{sub}$), 11/16 ($55/16x_{sub}$), 15/16 ($75/16x_{sub}$) for $y = 0.75$, see Table VI and Fig. 14. The calculations are in reasonable agreement with the experimental values considering that no attempt was made to perform a full profile analysis, see Table IV. However, in the context of the previous discussion, it seems likely that the actual atom locations are systematically displaced away from these ideal positions. A representation of this type of modulation, assuming simple sinusoidal displacements with a period $5a_{sub}$, is shown schematically in Fig. 14. For an ideal sine wave with $a = 5a_{sub}$ the displacements lead to two different cation–cation distances in the channels. More complex modulations would yield a range of inter-ion separations along the channels, which may be expected in a sample containing a noninteger ratio of aliovalent ions. The difference in the phase of the modulation along c is directly related to δc; for example, at $z_{subcell} = 1$ the displacive wave is retarded by $\delta c(2\pi)$, which for this composition corresponds to a phase lag of 0.4π.

The excellent agreement between the observed intensities and those calculated using the models described above gives further credence to the argument that the supercells of the incommensurate superstructures are

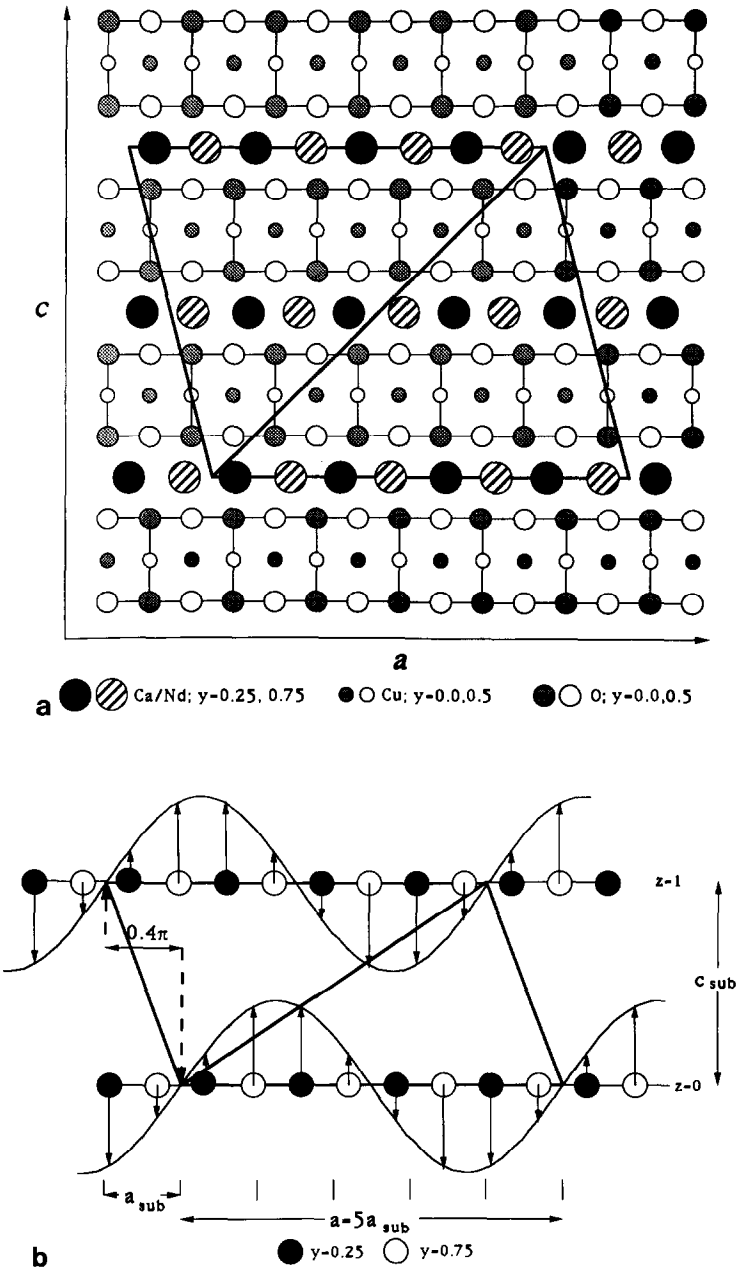

FIG. 14. (a) Schematic of proposed "ideal" monoclinic supercell for $Ca_{2.315}Nd_{1.685}Cu_5O_{10}$, $\delta a = \delta c = 0.2$. (b) Modulated displacements for the supercell in arbitrary units; for clarity the longitudinal displacements along a are represented by transverse displacements.

TABLE VI

IDEAL ATOM POSITIONS FOR $Ca_{2.315}Nd_{1.685}Cu_5O_{10}$

Atom	x	y	z	occup.
Cu1	0.35	0.5	0.75	1.0
Cu2	0.45	0.0	0.75	1.0
Cu3	0.75	0.5	0.75	1.0
Cu4	0.85	0.0	0.75	1.0
Cu5	0.95	0.5	0.75	1.0
Ca1	0.0625	0.25	0.0	0.58
Nd1	0.0625	0.25	0.0	0.42
Ca2	0.1875	0.75	0.0	0.58
Nd2	0.1875	0.75	0.0	0.42
Ca3	0.3125	0.25	0.0	0.58
Nd3	0.3125	0.25	0.0	0.42
Ca4	0.4375	0.75	0.0	0.58
Nd4	0.4375	0.75	0.0	0.42
O1	0.05	0.5	0.375	1.0
O2	0.15	0.0	0.375	1.0
O3	0.25	0.5	0.375	1.0
O4	0.35	0.0	0.375	1.0
O5	0.45	0.5	0.375	1.0
O6	0.55	0.0	0.375	1.0
O7	0.65	0.5	0.375	1.0
O8	0.75	0.0	0.375	1.0
O9	0.85	0.5	0.375	1.0
O10	0.95	0.0	0.375	1.0

Note. Space group $P2_1/c$, a = 14.138, b = 6.348, c = 15.554 Å, β = 136.65°.

based on similar idealized models and differ only through the period of the modulation along a^* and through the correlations along c^*. Consider the $P2_1/c$ monoclinic supercell for $Ca_2Y_2Cu_5O_{10}$, where $\delta a = 0.2$, $\delta c = 0.25$, and $\beta = 180° - \tan^{-1}[c \times \delta a/a(1 - \delta c)] = 134.9°$. The monoclinic supercell, which is incommensurate with the orthorhombic subcell, can be constructed by displacing the origin of the subcell at $z = 1$ by $\{[(1 - \delta c)/\delta a]a_{sub}\} = 3.75a_{sub}$, or for the alternative monoclinic setting by a displacement of $-[(\delta c/\delta a)a_{sub}] = -1.25a_{sub}$, see Fig. 15. If this superstructure simply involved equal $3.75a_{sub}$ displacements of the origin and the "ideal" cation positions in the channels, the new positions, at $z_{sub} = 1$ for example, would have x_{sub} = 5/16 + 3.75 = 65/16, 25/16 + 3.75 = 85/16, 45/16 + 3.75 = 105/16, and 65/16 + 3.75 = 125/16 for y 0.25; and 75/16, 95/16, 115/16, and 135/16 for $y = 0.75$. Because $\delta c = 0.25$ for this composition, the shift in the origin is equal to an integer number of ideal cation–cation distances and the new positions at $z_{sub} = 1$, and at all the other channel positions, are crystallographically equivalent to those at $z = 0$. Therefore, if the supercell formation only involved an equal displacement of the origin and the channel atom positions, the symmetry of the supercell would remain orthorhombic with $\delta a = 0.2$ and $\delta c = 0$, see Fig. 15. This "ideal" orthorhombic supercell, space group *Pnca*, is identical to that reported for $Ca_4Cu_5O_{10}$, where it may make sense for all the cation–cation distances to be identical. However, this simple atom arrangement cannot be correct for $Ca_2Y_2Cu_5O_{10}$, or $Ca_2(Nd,Gd)_2Cu_5O_{10}$, where the electron and X-ray patterns clearly support a supercell with monoclinic symmetry. Therefore, a simple uniform displacement of the ideal channel–cation positions cannot be responsible for the supercells observed in the ternary $NaCuO_2$-type compounds.

An alternative supercell, which does yield results consistent with those observed experimentally, can again be formulated by treating the ordering in terms of a displacive modulation, modeled for simplicity as a simple sine wave. As described above for the ideal model, the monoclinic symmetry of the cell can be generated by a displacement of the origin by $3.75a_{sub}$ at $z = 1$; for the displacive supercell this corresponds to a phase advance in the modulation wave by $(1 - \delta c)2\pi = 1.5\pi$, or correspondingly, a phase retardation of 0.5π, see Fig. 15(b). In this figure the ideal, equally separated cation sites are shown together with a sinusoidal modulation with period $a = 5a_{sub}$; the actual magnitude of the cation displacements from their "ideal" positions are unknown and have been illustrated in arbitrary units. As noted above, for a wave with zero ampli-

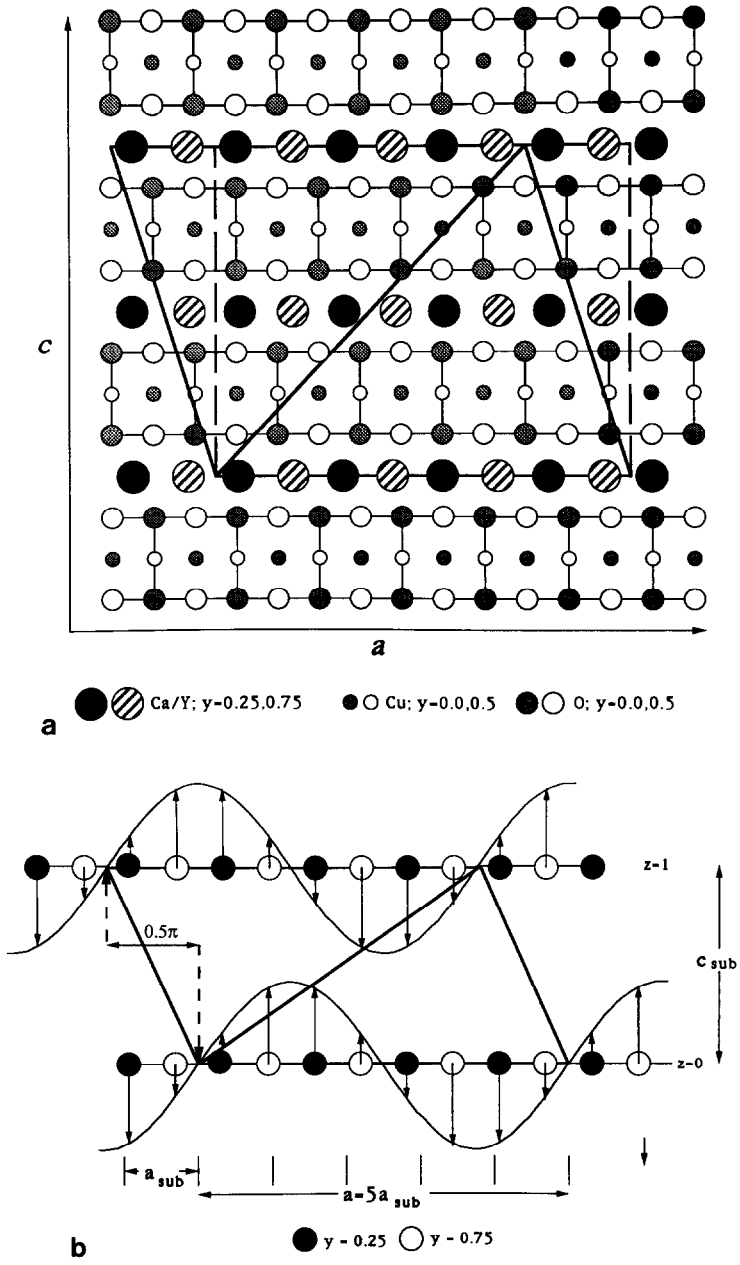

FIG. 15. Proposed supercell for $Ca_2Y_2Cu_5O_{10}$ with $\delta a = 0.2$ and $\delta c = 0.25$: (a) ideal positions for zero displacement; solid lines show monoclinic supercell, hatched line denotes "$Ca_4Cu_5O_{10}$-type" orthorhombic supercell. (b) Displacive modulation; longitudinal displacements along a are represented by transverse displacements.

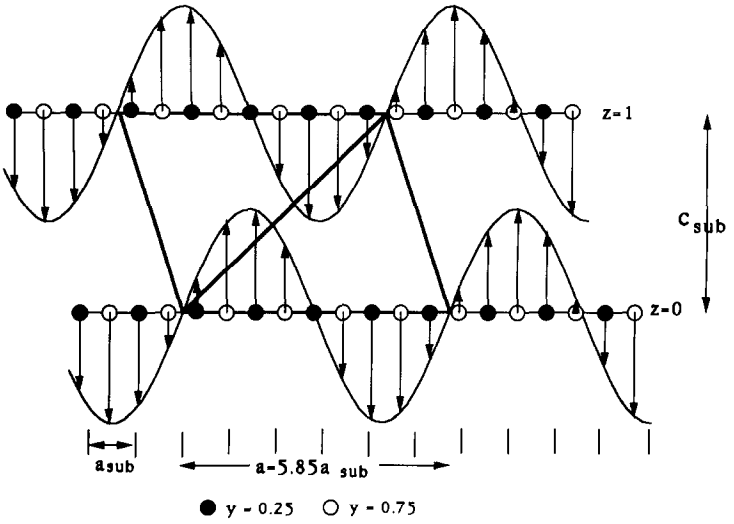

FIG. 16. Schematic of proposed displacements for $Ca_{2.75}Y_{1.25}Cu_5O_{10}$; $a = 5.85a_{sub}$, $\delta c = 0{\cdot}227$.

tude, i.e., zero displacement from the ideal positions, the cell symmetry is orthorhombic and "reduces" to that observed for $Ca_4Cu_5O_{10}$. Again a finite amplitude immediately leads to the nonuniform cation–cation separations that would be expected in these materials. Presumably in the ternary compounds the amplitude as well as the period of the modulation is dictated by the size, charge, and site preference of the channel ions. Although no detailed high resolution TEM observations were made in this work, the lattice fringe images presented in Figs. 6 and 7 perhaps lend some direct support these models. The substantial disorder along c makes any structural analysis difficult; however, in several regions of the [010] images direct measurement of the (h00) fringe contrast confirmed a nonuniform spacing along a. It is recognized that these images cannot lead to a direct confirmation of the atomic locations and do not allow any detailed structural interpretation, but they certainly do not contradict the analysis presented above.

Representation of the superstructures of all the $Ca_{2+x}M_{2-x}Cu_5O_{10}$ compounds in terms of a displacive modulation gives a satisfactory interpretation of the sensitivity of the period of the superstructure to both the $Ca:M^{3+}$ content and to the chemistry of M^{3+}. In all three solid solutions, as the trivalent ions are substituted by Ca the period of the modulation along a increases rapidly. For example, with M = Y at $x = 0.75$, $a = 5.848a_{sub}$; a schematic of a possible modulated superstructure for this phase, where $\delta c = 0.227$ and the modulation at $z_{sub} = 1$ is advanced by 1.546π, is shown in Fig. 16. The increase in the periodicity reflects the changes in the equilibrium atom separations as the trivalent ions are removed from the system. This type of order also gives a satisfactory interpretation of the variation of δa with M at a given value of x. For example, when $x = 0.315$, for M = Y, $a = 5.348a_{sub}$ (and $\delta c = 0.248$); but for M = Nd, $a = 5a_{sub}$ and $\delta c = 0.2$. These changes in the periodicity presumably reflect the different equilibrium ion separations which result from the different size and site preference of the trivalent ions in the two systems.

Finally, although the chemistry of M^{3+} affects the periodicity of the supercells

along both a and c, changes in the chemistry of the divalent ion only seem to perturb the correlation along c. In Sr-doped solid solutions with $(Ca_{2-z}Sr_z)Nd_2Cu_5O_{10}$ the periodicity of the supercells along a are unaffected by the Sr-doping, whereas the correlations along c are very sensitive to the value of z. The insensitivity of the modulation along a to this substitution may again highlight the importance of the trivalent positions in "pinning" the period of the displacive wave along the channels, with the change in the size of the divalent ions only perturbing the c correlations, which are presumably dependent upon a series of more complex 2nd or 3rd nearest neighbor interactions.

Conclusions

Solid solutions with structures based on an orthorhombic "$NaCuO_2$-type" subcell are formed over a wide range of composition in the CaO–M_2O_3–CuO systems, M = Y, Nd, Gd. These structures contain infinite one-dimensional chains of edge-shared square planar cuprate groups crosslinked by the larger cations which occupy sites in the inter-chain tunnels. Samples with $Ca/M \geq 1$ have the stoichiometry $Ca_{(2+x)}M_{(2-x)}Cu_5O_{10}$; the maximum solubility range corresponds to $x = 0.8$, 0.4, and 0.3 for M = Y, Gd, and Nd, respectively. Single phase samples with $Ca/M < 1$ are also formed in the Gd and Nd systems; these have the stoichiometry $M_{(10/3-y)}Ca_{(3y/2)}Cu_5O_{10}$, with $5/6 \leq y \leq 4/3$ for Nd and $1.13 \leq y \leq 1.33$ for Gd. For the Ca-rich samples the extent of solid solubility appears to vary with the specific site preference of the trivalent ion, whereas for the trivalent-rich compositions the solubility limit is a direct function of the size of M. Long-range ordered arrangements of the inter-chain ions lead to the formation of superstructures whose symmetry and periodicity is a sensitive function of the $Ca : M^{3+}$ ratio and the size of M. In general, the superstructures are monoclinic and incommensurate along, and perpendicular to the cuprate chains. The ordering can be described in terms of a periodic displacive modulation of the inter-chain cations from their "ideal," equally spaced positions. Models for the displacement based on a simple sinusoidal modulation give excellent agreement with the experimental diffraction profiles collected using X rays and electrons.

Acknowledgments

This work was supported by the National Science Foundation under grants DMR-88-19027 and DMR 88-19885 through the University of Pennsylvania MRL program. Thanks also go to Elizabeth Caignol and Todd King for sample preparations and X-ray work.

References

1. P. K. Davies, E. Caignol, and T. King, *J. Am. Ceram. Soc.* **74,** 569 (1991).
2. T. Siegrist, R. S. Roth, C. J. Rawn, and J. J. Ritter, *Chem. Mater.* **2,** 192 (1990).
3. N. E. Brese, M. O'Keeffe, R. B. Von Dreele, and V. G. Young, *J. Solid State Chem.* **83,** 1 (1989).
4. J. Pickardt, W. Paulus, M. Schmalz, and R. Schollhorn, *J. Solid State Chem.* **89,** 308 (1990).
5. H. Müller-Buschbaum, *Angew. Chem. Int. Ed. Engl.* **16,** 674 (1977).
6. K. Hestermann and R. Hoppe, *Z. Anorg. Allg. Chem.* **367,** 261 (1969).
7. K. Hestermann and R. Hoppe, *Z. Anorg. Allg. Chem.* **367,** 249 (1969).
8. K. Wahl and W. Klemm, *Z. Anorg. Allg. Chem.* **270,** 69 (1952).
9. H. D. Wasel-Nielen and R. Hoppe, *Z. Anorg. Allg. Chem.* **375,** 43 (1970).
10. R. S. Roth, C. J. Rawn, J. J. Ritter, and B. P. Burton, *J. Am. Ceram. Soc.* **72,** 1545 (1989).
11. P. K. Davies and A. Navrotsky, *J. Solid State Chem.* **46,** 1 (1983).
12. R. D. Shannon, *Acta Crystallogr., Sect. A: Found. Crystallogr.* **32,** 751 (1976).